Kinetic Modeling of the Polymer-Derived Ceramics Route: Investigation of the Thermal Decomposition Kinetics of Poly[*B*-(methylamino)borazine] Precursors into Boron Nitride

Samuel Bernard,*,† Koffi Fiaty,‡ David Cornu,† Philippe Miele,† and Pierre Laurent‡

Laboratoire des Multimatériaux et Interfaces (UMR 5615 CNRS) et Laboratoire d'Automatique et de Génie des procédés (UMR 5007 CNRS), 69622 Villeurbanne, France

Received: October 19, 2005; In Final Form: March 14, 2006

A complete kinetic modeling of the polymer-derived ceramics (PDCs) route is achieved for the first time through the investigation of the solid-state decomposition of a typical melt-spinnable poly[*B*-(methylamino)-borazine] into boron nitride fibers at various heating rates. Through the use of the Lorentz fitting approach, it is shown that the two-step weight loss associated with the polymer-to-ceramic conversion is governed by a complex interplay of five diffusion-type transport mechanisms that are independent of the applied heating schedule. The application of the Friedman method to dynamic thermogravimetry data yields E_a and ln A values that are seen to increase with the extent of the ceramic conversion from region one ($E_a = 38.73$ kJ mol^{-1}) to region five ($E_a = 146.64$ kJ mol^{-1}). This fact indicates that both the mechanisms within those regions are parallel routes to the formation of the final solid-state material and their complexity increases with the conversion progress. The cross-linking process (first weight loss) of the polymer is governed by three dependent poorly energetic mechanisms. The first weight loss is activated by ammonolysis reactions that provide a modified polymer capable of undergoing condensation reactions in regions two and three to yield a highly cross-linked polymer. A large evolution of methylamine is identified during this process. Mineralization (region four) and ceramization (region five) steps are represented by two highly energetic multistep mechanisms. The mineralization step is associated with a large evolution of methylamine and occurs during the transition between the cross-linking and ceramization processes through the cleavage of the interring B−N bonds. Ceramization represents the end of the polymer-to-ceramic conversion in which the planar consolidation of BN hexagons occurs through complex structural rearrangements of the borazine units (cleavage of the intraring B−N bonds) accompanied with an ammonia evolution. Finally, the simulation of the polymer-to-ceramic conversion was demonstrated through a simplified model that appropriately predicted experimental data.

Introduction

Preceramic polymers represent oxygen-free inorganic/organometallic systems that provide non-oxide ceramics with a tailored chemical composition and a closely defined nanostructural organization by proper thermal treatment (curing and thermolysis processes) under controlled atmospheres.[1−5] Decomposition of such polymers can be described as a simple solid-state process according to eq 1.

$$\text{polymers (s)} \rightarrow \text{ceramics (s)} + \text{species (g)} \qquad (1)$$

This polymer-derived ceramics (PDCs) route is an emerging chemical process as attested by the increasingly commercial development of preceramic polymers (KiON Ceraset Polysilazane, PCS, PHPS[6−8]) to produce near-net shapes in a way not known from other techniques.

It is recognized that the synthesis of such solid-state PDCs must be performed with the greatest precision to maintain a high level of performance. For example, because the structure and composition of polymers determine the structure and performances of ceramics, detailed investigations of their molecular chemistry are required. In addition, the control of the polymer-to-ceramic conversion through the design of the intermediate steps (to convert the polymer system into an inorganic intermediate) and the use of annealing treatments (to change the inorganic intermediate into the desired final nanostructure) must be done with full understanding to generate materials capable of performing in demanding conditions. In a general way, the identification of mechanisms is performed by thermogravimetry (TG) analyses coupled with mass spectrometry (MS).[9−11] Unfortunately, these techniques do not constitute a complete diagnostic tool, since the combination of such data only offers a basic representation of some mechanisms. Therefore, serious doubts arise about an accurate description of the polymer-to-ceramic conversion by using only such techniques. A kinetic approach to eq 1 in complement to TG and MS data could offer a greater insight into the elucidation of mechanisms as the solid changes from the polymer to the ceramic state. The knowledge of overall kinetic parameters should improve the quality of ceramic products.

Kinetics of solid-state process have most often been based on a specific rate equation (eq 2) using common methods including TG and differential TG (DTG) techniques[12−26]

$$\frac{d\alpha}{dt} = A \exp\frac{-E_a}{RT} f(\alpha) \qquad (2)$$

where α is the fractional conversion, A is the preexponential

* Author to whom correspondence should be addressed. Phone: +33 472 433 612. Fax: +33 472 440 618. E-mail: Samuel.Bernard@univ-lyon1.fr.

† Laboratoire des Multimatériaux et Interfaces.

‡ Laboratoire d'Automatique et de Génie des Procédés.

10.1021/jp055981m CCC: $33.50
Published on Web 04/14/2006

TABLE 1: Algebraic Expressions for the $f(\alpha)$ and $g(\alpha)$ Functions for the Most Frequently Cited Mechanisms in Solid-State Processes

symbol	$f(\alpha)$	$g(\alpha)$	mechanism
F_1	$(1-\alpha)$	$-\ln(1-\alpha)$	first-order reaction (random nucleation)
F_n	$(1-\alpha)^n$	$1/n[1-(1-\alpha)^{-(n-1)}]$	generalized *n*th-order reaction
P_1	$\alpha(1-\alpha)$	$\ln[\alpha/(1-\alpha)]$	Prout−Tompkins model
A_n	$n(1-\alpha)[-\ln(1-\alpha)]^{1-1/n}$	$[-\ln(1-\alpha)]^{1/n}$	nucleation and growth (Johnson−Mehl−Avrami equation; JMA)
R_1	1	α	phase-boundary-controlled reaction (one-dimensional movement)
R_2	$(1-\alpha)^{1/2}$	$2[1-(1-\alpha)^{1/2}]$	phase-boundary-controlled reaction (contracting area)
R_3	$(1-\alpha)^{2/3}$	$3[1-(1-\alpha)^{1/3}]$	phase-boundary-controlled reaction (contracting volume)
D_1	$^1/_2\alpha$	α^2	one-dimensional diffusion
D_2	$1/[-\ln(1-\alpha)]$	$(1-\alpha)\ln(1-\alpha)+\alpha$	two-dimensional diffusion (bidimensional particle shape)
D_3	$3(1-\alpha)^{2/3}/2[1-(1-\alpha)^{1/3}]$	$[1-(1-\alpha)^{1/3}]^2$	three-dimensional diffusion (Jander equation)
D_4	$3/2[(1-\alpha)^{-1/3}-1]$	$(1-{}^2/_3\alpha)-(1-\alpha)^{2/3}$	three-dimensional diffusion (Ginstling−Brounshtein equation)

factor, E_a is the activation energy (J mol^{-1}), R is the gas constant ($R = 8.314$ J K^{-1} mol^{-1}), and T is the absolute temperature in Kelvin. $f(\alpha)$ represents a reaction model related to the mechanism.

Although there are no reports concerning the kinetics of eq 1 using eq 2, the curing and thermolysis processes of preceramic polymers yielding ceramic products represent a non-isothermal heating procedure generating weight losses, which clearly justifies the application of eq 2 to preceramic systems.

The present paper therefore reports for the first time a general kinetic view of the PDCs preparation using eq 2 that could be applied to a large variety of polymers in a wide range of compositions, processed forms, and sizes. This article is exclusively focused on the determination of kinetic parameters and the prediction of solid-state mechanisms in terms of the physics and chemistry associated with the thermal decomposition of a poly[*B*-(methylamino)borazine].

With definite physical and chemical characteristics, poly[*B*-(methylamino)borazine] may represent a melt-spinnable preceramic polymer that is ideally suited for preparing boron nitride fibers by curing and thermolysis processes of green fibers up to 1800 °C.[27] Previous studies have demonstrated that the mechanical and structural properties of boron nitride fibers were closely related to the controlled achievement of the two-step weight loss from 25 to 1000 °C.[27]

Kinetic modeling data of non-isothermal TG analyses at various heating rates are therefore proposed in the present paper for a typical melt-spinnable poly[*B*-(methylamino)borazine]. This allows us to obtain fundamental insight into the ceramic transformation process, and therefore to aid reactor design, process development, and optimization for the preparation of boron nitride fibers.

Data Analysis

In gaseous-state processes, it is widely shown that a typical rate expression for a conventional chemical reaction is proportional to the concentration of reactant molecules ($[M_r]$) as represented by the differential rate law in eq 3[28]

$$-\frac{d[M_r]}{dt} = k[M_r]^n \tag{3}$$

where n is the order of the reaction.

In contrast, eq 2 (Introduction) showed that the heating of a preceramic solid represented by a solid-state reaction uses the fractional conversion α ($0 \le \alpha \le 1$) as the extent of ceramic conversion instead of $[M_r]$. The fractional conversion may be defined as the ratio of actual weight loss to total weight loss corresponding to a given step of the decomposition

$$\alpha = \frac{(W_o - W)}{(W_o - W_f)} \tag{4}$$

where W, W_o, and W_f are the actual, initial, and final weights of the polymer, respectively.

It should be emphasized that the Arrhenius equation $k = A \exp -E_a/RT$ has been generally accepted and successfully applied to numerous reactions involving solids. Its application is justified by different arguments than those for homogeneous gas-phase systems.[29,30]

Activation Energy. The fractional conversion α may be modeled either by fitting to known solid-state reaction models or by using a model-free approach. The latter including the Friedman and Kissinger methods allows the best explanation for most solid-state reactions.

The Kissinger method was investigated for experimental DTG curves in the present paper.[31] This differential method is widely used in solid-state reactions, since the value of E_a can be determined without a precise knowledge of the reaction mechanism

$$\ln \frac{b}{T_m^2} = \ln\left[\frac{AR}{E_a}\left(\frac{df(\alpha)}{d\alpha}\right)\right] - \frac{E_a}{R}\left(\frac{1}{T_m}\right) \tag{5}$$

The Kissinger method is based on both the differentiation of eq 2 and the temperature where the rate of weight loss is maximum (T_m) in DTG curves. Activation energies E_a can be obtained from the slope of the straight line resulting from the plot of $\ln b/T_m^2$ versus $1/T$.

In comparison, the activation energies E_a were extracted from simulated DTG data using the popular multiscan Friedman method (isoconversional approach) taking the logarithm form of eq 2 after rearranging terms and assuming the validity of the Arrhenius equation (eq 5)[32]

$$\ln \frac{d\alpha}{dt} = \ln f(\alpha) + \ln A - \frac{E_a}{RT} \tag{6}$$

For a fixed value of α, the first and the second terms in the right-hand side of eq 5 are constant. Hence, the plot of $\ln d\alpha/dt$ as a function of $1/T$ from data at various heating conditions can be correlated by the least-squares method to yield straight lines with the slope $-E_a/R$ without knowledge of $f(\alpha)$.

Mathematical Expression of Mechanisms. The objective of the kinetic modeling lies in the determination of a $f(\alpha)$ function, termed the differential kinetic function (Table 1[21−23]), which must fulfill the mathematical requirement of eq 2 (Introduction).

The simple kinetic models reported in Table 1 are mostly derived on the basis of a formal physical description of a single reaction mechanism (physical-geometrical assumptions of regularly shaped bodies). However, it is rational to assume that these numerical models may accommodate the complex solid-state reactions with multiple steps using an appropriate deconvolution method where each isolated region is controlled by its own rate-limiting reaction. An appropriate deconvolution of the experimental DTG curves allows the range for α to be restricted within regions corresponding to the kinetics for each individual stage and therefore the complexity of the process to be readily discovered. Hence, within these limits, the derivatives for the individual stage can be distinguished from each other, and the overall kinetic curves coincide with one of the corresponding partial kinetic curves. Each mechanism may be therefore individually treated by the specific reaction models reported in Table 1.

The $f(\alpha)$ function can be extracted from both the knowledge of E_a and the recorded TG data using the methods introduced by Málek et al.[19]

First, the authors described a reference equation based on the decomposition rate $d\alpha/dt$, which is derived in the form of a special factor $y(\alpha)$ proportional to the $f(\alpha)$ function by simply plotting the term $d\alpha/dt \exp(x)$ ($x = E_a/RT$) as a function of α

$$y(\alpha) = \left(\frac{d\alpha}{dt}\right) \exp(x) = Af(\alpha) \tag{7}$$

The curve profiles of some common $y(\alpha)$ functions versus α were published elsewhere.[19]

According to the shape of the as-plotted curves, the $f(\alpha)$ function for the related mechanism may be deduced. However, it is important to mention here that the kinetic parameters can deviate from the true values as a simple mathematical consequence of eq 2 due to the complexity of the reaction. Therefore, TG curves cannot be only described by the $f(\alpha)$ function.[33,34]

According to the expected complexity of the polymer-to-ceramic conversion, we have considered the Master plot method as an alternative route to eq 7.

The Master plot method consists of the introduction of an empirical function $z(\alpha)$ defined by eq 8 containing the smallest possible number of constancy leading to some flexibility sufficient to describe the real process as closely as possible

$$z(\alpha) = \frac{1}{b}\left(\frac{d\alpha}{dt}\right)\pi(x)T = f(\alpha)g(\alpha) \tag{8}$$

where $\pi(x)$ ($x = E_a/RT$) is an approximation of the temperature integral and $g(\alpha)$ represents the integral of $1/f(\alpha)$, termed the integral kinetic function (Table 1).[19]

The method is based on the comparison of Master plots, i.e., reference curves, (Figure 1) using the definitions of $f(\alpha)$ and $g(\alpha)$ for every one of the models reported in Table 1 with the experimental curves obtained by plotting $1/b(d\alpha/dt)\pi(x)T$ as a function of α.

The $y(\alpha)$ and $z(\alpha)$ functions display each maximum α_y^∞ and α_z^∞ values for every one of the kinetic models.[19]

Because the $y(\alpha)$ and $z(\alpha)$ functions should be invariable with respect to temperature or heating rate, the combination of the curve shape with the values of α_y^∞ and α_z^∞ allows the most appropriate kinetic models included in Table 1 to be determined for each individual decomposition stage. It should be mentioned that under dynamic conditions, the shapes of $y(\alpha)$ and $z(\alpha)$ strongly depend on E_a. As a consequence, such functions should be normalized within the [0,1] conversion range.

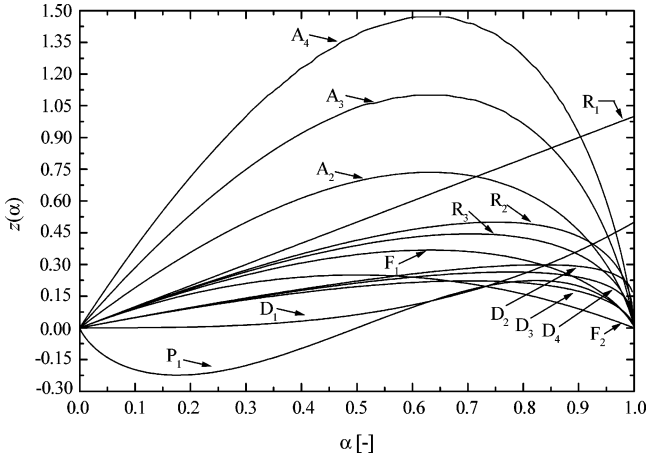

Figure 1. Reference curves representing the plot of the $z(\alpha)$ function vs α for the most cited kinetic models in solid-state reactions.

Preexponential Factor and Validity of the Postulated Mechanisms. The Friedman method was also used for the evaluation of $\ln A$ from the plot of $\ln A + \ln f(\alpha)$ as a function of the *y*-intercept of the straight lines representing the plot of $\ln d\alpha/dt$ as a function of $1/T$ (eq 5).[32]

To provide a complete kinetic view, the reliability of $\ln A$ was also checked using an alternative method based on the second derivative of α (second-derivative method,[19] eq 9). The preexponential factor *A* (eq 9) may be obtained for every mechanism from the derivative of $f(\alpha)$, $f'(\alpha)$, assuming the validity of $f(\alpha)$[19]

$$A = -\frac{bx_p}{f'(\alpha_p)T_m}\exp(x_p) \tag{9}$$

The application of the above-described methods is illustrated in the present paper for a non-isothermal decomposition of a typical melt-spinnable poly[*B*-(methylamino)borazine] into a solid-state boron nitride product. To our knowledge, this paper describes the first application of these methods for the preparation of PDCs. Above all, they allow, for the first time, the activation energy and preexponential factor to be evaluated as well as the physical chemistry aspect of the reaction mechanisms involved in the polymer-to-ceramic transformation process to be known.

Experimental Section

It should be mentioned that the temperatures were expressed in Kelvin for consistency and homogeneity with the kinetic analysis.

Polymer synthesis was carried out in a purified argon atmosphere using standard Schlenk manipulations and argon/vacuum lines. Nitrogen and ammonia (>99.999%) were used in the as-received state.

Materials. The air- and moisture-sensitive solid-state polymer, the poly[*B*-(methylamino)borazine], was prepared by thermolysis at 453 K through condensation reactions of a molecular precursor, the *B*-(methylamino)borazine, according to a well-established procedure.[35]

The elemental analyses were performed using various apparatus at the Service Central de Microanalyses du CNRS (Vernaison, France). Found (wt %): C, 19.1; H, 7.3; N, 49.0; B, 24.6. Anal. calcd (wt %): C, 14.9; H, 6.2; N, 52.1; B, 26.8. NMR measurements were performed in solution on a Bruker AM 300 spectrometer run at 300 MHz for ^{1}H, 96.29 MHz for ^{11}B, and 75 MHz for ^{13}C. Tetramethylsilane was used as a

reference. ^{1}H NMR (CD_2Cl_2, ppm): 1.86 br (N(*H*)CH_3), 2.47 vbr (N(H)C*H*$_3$), 2.55 vbr (NC*H*$_3$), 2.64−3.37 br (N*H* borazine). ^{11}B NMR (C_6D_6, ppm): 25.77 br. ^{13}C NMR (CD_2Cl_2, ppm): 27.6, 27.9 (N(H)*C*H_3), 31.2 (N*C*H_3, CH_3 bridges). The IR spectrum was recorded as a KBr pellet in the wavenumber range 4000−400 cm^{-1} using a Nicolet Magna 550 Fourier transform infrared (FT-IR) spectrometer. IR (KBr, cm^{-1}): 3438 (m, ν(N−H)); 2954 (w), 2920 (w), 2894 (w), 2816 (m) (ν(C−H)); 1605 (s, δ(N(H)CH_3)); 1515 (s, ν(B−N)); 1105 (s, ν(C−N); 702 (w, out-of-plane B−N ring).

Sample Preparation. Preparation of the samples was conducted using an inert-gas glovebox purified and dried with phosphorus pentoxide. The sample was ground up into a fine powder before being introduced into the cylindrical frame of the TG apparatus. Special precautions were taken while running the experiments to prevent exposure to air or moisture. In particular, the sample-furnace area was purged two times immediately after the sample introduction to limit oxygen contamination, before starting the TG experiments.

Techniques. The thermal decomposition of the polymer was followed by TG experiments (TGA 92 16.18 by Setaram) under different heating dynamic schedules. Six separated heating rates *b* of 0.8, 1.6, 3.2, 6.4, 13, and 20 K min^{-1} were applied. Each run was carried out in duplicate for averaging and consistency.

The experiments were performed in the dynamic mode in a mixed ammonia and nitrogen atmosphere (1:1) from 298 to 1273 K, then continued in a nitrogen atmosphere in the temperature range 1273−1773 K using platinum crucibles (sample weight ∼40 mg) at ambient atmospheric pressure. Nitrogen was combined with ammonia from 298 to 1273 K to protect the balance chamber against corrosion due to the use of the reactive ammonia gas.

The gaseous byproducts produced during TG experiments were identified in a continuous process by gas chromatography (Hewlett-Packard model Agilent micro-GC M200) coupled with a quadripole mass spectrometer (Agilent 5973 Network Mass Selective Detection). Species were identified on the basis of their MS molecular ion peaks and by comparison of their gas chromatography (GC) retention times to those known for the gases (hydrogen, ammonia, methylamine, dimethylamine, nitrogen, argon, and oxygen). A quantitative GC analysis has been carried out from the area of the signals corresponding to the identified gas.

Results

Experimental Curves. The reaction depicted in eq 1 is analyzed through the transformation of a typical melt-spinnable poly[*B*-(methylamino)borazine] ($T_{synthesis}$ = 453 K; solid-state polymer) into boron nitride (solid-state ceramic material). Figure 2 presents a set of six experimental curves that plots the gradual increase of the fractional conversion α of the poly[*B*-(methylamino)borazine] as a function of the temperature, yielding a boron nitride residue at 1773 K. These curves are generated in a combined way by means of weight loss measurements recorded during experiments at various heating rates ranging from 0.8 to 20 K min^{-1} in a mixed ammonia and nitrogen atmosphere (298−1273 K), then in a nitrogen atmosphere (1273−1773 K) using eq 4. It should be mentioned that we use ammonia as a selected reactive atmosphere, because it (i) acts as an efficient curing agent and (ii) allows the carbon-based pendent groups in the polymer structure ($[B_{3.0}N_{4.6}C_{2.1}H_{9.5}]_n$, $n \approx 7$) to be removed and a carbon-free boron nitride product with an improved crystallization tendency to be generated at 1773 K (C/B/N = 0:1.2:1).[35]

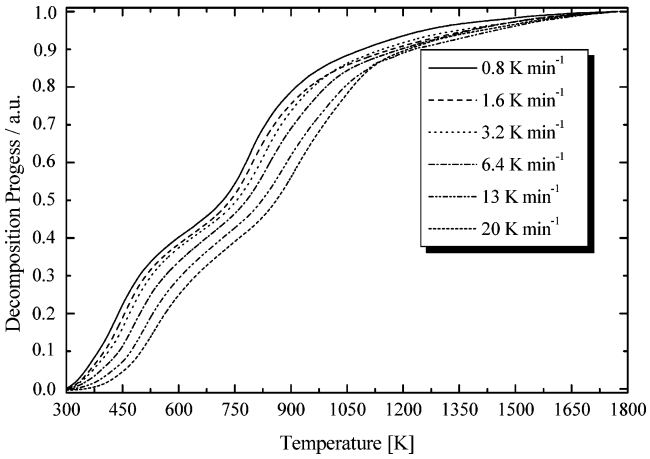

Figure 2. Decomposition curves of a typical melt-spinnable poly[*B*-(methylamino)borazine] as a function of temperature deduced from TG data for six heating rates in a mixed ammonia and nitrogen atmosphere (298−1273 K), then in a nitrogen atmosphere (1273−1773 K).

It is known that the thermal decomposition of poly[*B*-(methylamino)borazine] proceeds in a two-step weight loss yielding a ceramic yield that approaches 54% (b = 0.8 K min^{-1}) depending on the molecular weight of the used polymer.[35] By conversion of the weight loss data *W* into the fractional conversion α through eq 4, Figure 2 shows that the decomposition proceeds in the intervals α [0−0.45] and [0.45−1] using the above-mentioned heating rates.

The thermal decomposition is strongly dependent on the heating dynamic schedule, since the experimental curves are shifted to higher temperatures as the heating rate increases from 0.8 to 20 K min^{-1}. Nevertheless, it is relevant to mention that the absence of changes in the curve profile suggests the occurrence of identical mechanisms whatever the applied heating rate. Gas chromatography analyses coupled in a continuous process with TG experiments highly reflected such observations.

As an illustration, it is shown that the nature of the gaseous byproducts identified during the thermal decomposition of the poly[*B*-(methylamino)borazine], namely, methylamine (CH_3-NH_2), is not changed using the different heating schedules. Moreover, the transformation of the polymeric network into the related inorganic material is characterized by a two-step evolution of methylamine, and despite an expected shifting of the evolution curves to higher temperatures, the two-region curve profile is retained with the increased heating rate (Figure 3).

These observations point to the fact that volatilization of low-molecular-weight boron-containing species (evaporation of polymer fragments) due to chain scission and back-biting, which could be considered with such low-molecular-weight polymers[36] ($M_w \approx$ 800−1300 g mol^{-1}), is avoided as the heating rate increases. This is an important requirement for an accurate kinetic analysis, since this indicates both that the amount of boron remains constant during decomposition and that the mathematical form of $f(\alpha)$ is expected to be independent of the applied heating rate during TG experiments.

The respective steps in the two temperature regions identified in both TG and GC experiments are recognized by the two emerging peaks representing the maxima of the decomposition rate as a function of temperature in DTG curves (Figure 4).

As supported by TG experiments, an increased heating rate shifts the temperatures corresponding to the maximum rate of decomposition, T_m, to higher values but did not involve any change in the curve profile and therefore in the mechanism of decomposition.

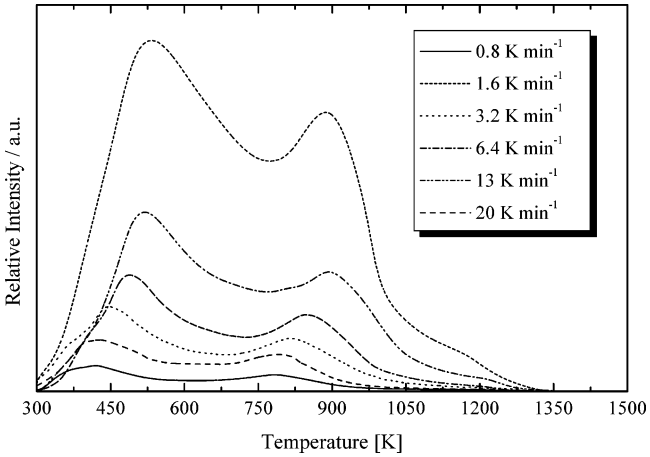

Figure 3. Evolution curves for methylamine identified by GC as a function of temperature during the thermal decomposition of the poly-[*B*-(methylamino)borazine] up to 1773 K for six heating rates.

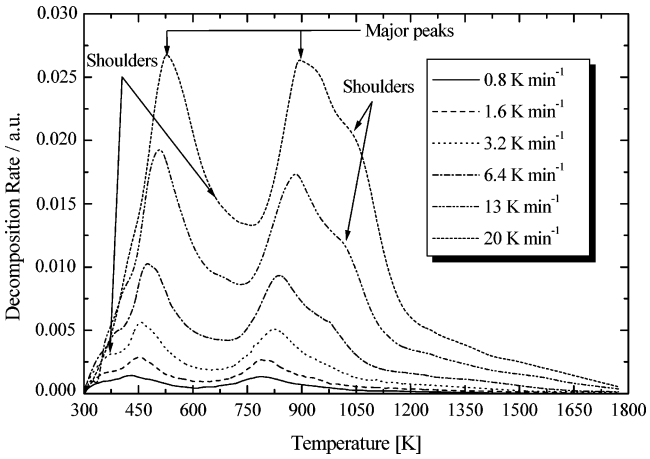

Figure 4. Decomposition rate of the poly[*B*-(methylamino)borazine] as a function of the temperature for six heating rates in a mixed ammonia and nitrogen atmosphere (298−1273 K), then in a nitrogen atmosphere (1273−1773 K).

TABLE 2: Temperature (T_m) for Every Maximum of the Decomposition Rate at Different Heating Rates and Activation Energies Associated with the Two Weight Losses

	T_m (K)	
heating rate (K min^{-1})	first peak (first weight loss)	second peak (second weight loss)
0.8	422.5	776.6
1.6	442	788.4
3.2	459	828.3
6.4	473	841
13	505.4	888
20	529	620
activation energy (E_a; kJ mol^{-1})	50.0	121.2

Interestingly, the shifting in the position of the peaks with heating rate contains information about the activation energy for the reactions using the Kissinger method.[31] Table 2 reports the values for each maximum (T_m) and the values of E_a of the corresponding mechanisms deduced from the plot of ln b/T_m^2 versus $1/T_m$ for each heating rate.

Significant differences in slopes and therefore in E_a values are seen going from the first weight loss to the second one. Table 2 shows that the first weight loss is associated with a poorly energetic process ($E_{a_1} = 50.0$ kJ mol^{-1}), whereas a highly energetic process ($E_{a_2} = 121.2$ kJ mol^{-1}) characterizes the second weight loss. However, the appearance of small shoulders on the left and right sides of the first peak in the DTG curves

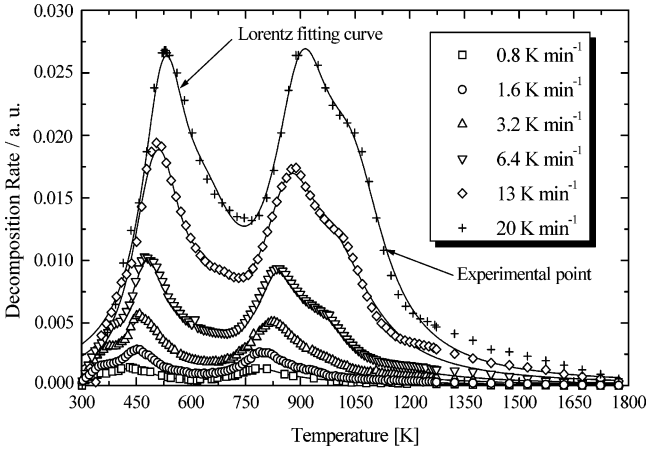

Figure 5. Lorentz fitting simulation of the experimental curves plotting the decomposition rate as a function of the temperature at every heating rate.

(Figure 4) suggests that these major stages are accompanied by nondiscernible (minor) stages. Shoulders also appear on the right side of the second peak for every one of the heating rates. Taken together, these facts suggest that the thermal decomposition of poly[*B*-(methylamino)borazine] includes an extremely complex sequence of superimposed solid-state mechanisms that cannot be separated in a clear temperature range based on experimental TG, DTG, and GC experiments.

The existence of a complicated decomposition progress with chemical reactions taking place simultaneously and/or successively increases the possibilities for making significant errors in fitting kinetic data and could lead to erroneous conclusions about the reaction models. To overcome the ambiguous evaluation of reaction identification when the poly[*B*-(methylamino)-borazine] changes into boron nitride, the experimental curves reported in Figure 4 have to be deconvoluted. Therefore, we have used a computational procedure based on both the data analysis program Origin 7.0 and an appropriate nonlinear fitting curve model to distinguish the individual stages from each other.

Application of the Lorentz Distribution to Experimental Curves. An examination of Figure 5 shows that the Lorentz function is the best method to fit the experimental data representing the decomposition rate of poly[*B*-(methylamino)-borazine] as a function of temperature.

The Lorentz (also known as Breit−Wigner, eq 10) distribution is a generalized form originally introduced to describe the cross-section of resonant nuclear scattering, which was derived from the transition probability of a resonant state with a known lifetime[37]

$$\frac{d\alpha}{dt} = \left(\frac{\omega}{2}\right)\frac{4}{4\pi[(T - T_m)]^2 + \omega^2} \qquad (10)$$

where ω is the full width at half-maximum (fwhm) of the Lorentz function.

It is relevant to mention here that it has been checked that eq 10 well describes the shape of every one of the kinetic models included in Table 1.

Interestingly, stages can be easily deconvoluted by increasing or decreasing the heating rate using the multiple-peaks Lorentz fitting method. As an illustration, the Lorentz-type curves reported in Figure 5 are mainly based on five Lorentz fitting peaks as accurately illustrated in Figures 6 and 7 for a thermal decomposition at 0.8 and 6.4 K min^{-1}, respectively. It should

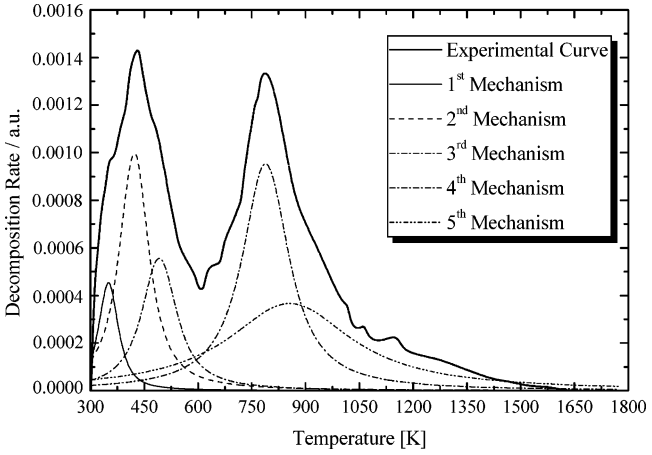

Figure 6. Simulation of the experimental DTG curve (0.8 K min^{-1}) using five Lorentz peaks.

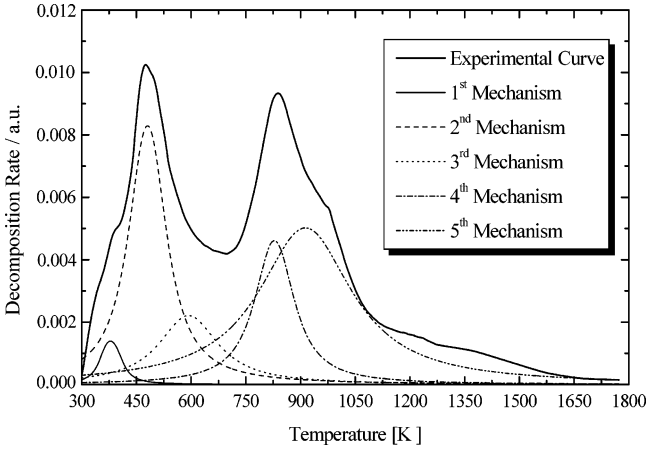

Figure 7. Simulation of the experimental DTG curve (6.4 K min^{-1}) using five Lorentz peaks.

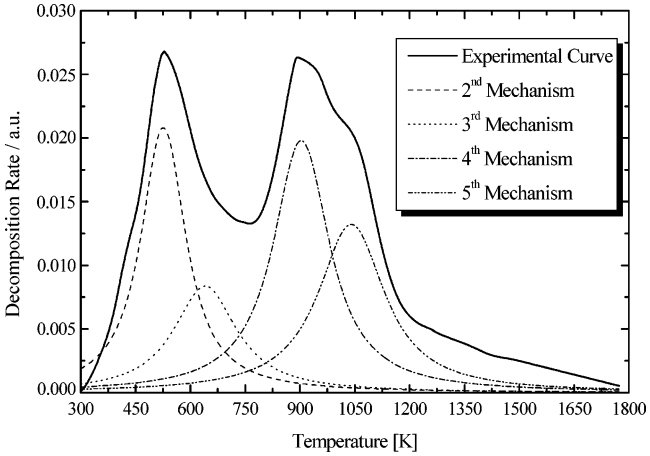

Figure 8. Simulation of the experimental DTG curve (20 K min^{-1}) using four Lorentz peaks.

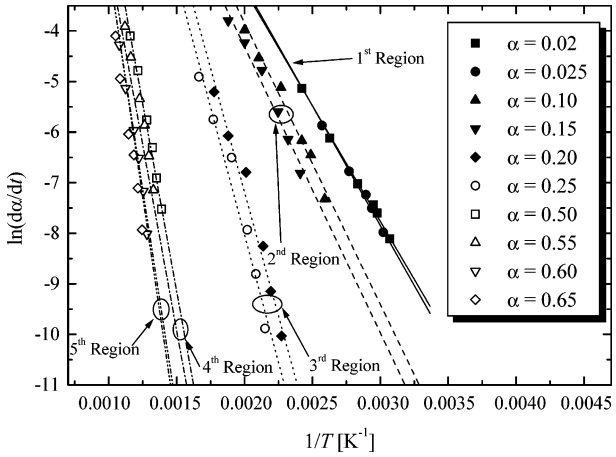

Figure 9. Determination of E_a as a function of α using the Friedman method for every one of the simulated regions.

be mentioned that five such Lorentz fitting peaks also really match experimental DTG curves recorded at 1.6, 3.2, and 13 K min^{-1}.

However, the deconvolution is clearly disturbed as the heating rate reached 20 K min^{-1} due to the existence of fully overlapping reactions at certain temperature ranges. As an illustration, the first and second peaks in Figures 6 (0.8 K min^{-1}) and 7 (6.4 K min^{-1}) are treated as an unique composite peak in Figure 8 (20 K min^{-1}). This probably means that the first stage, which shifts faster than others, is associated with the lowest activation energy.

Despite the presence of a nondiscernible region in the low-temperature regime at 20 K min^{-1}, it is reasonable to assume that the thermal decomposition of poly[*B*-(methylamino)-borazine] may be analyzed through a process that is composed of five stages: three regions for the first weight loss and only two for the second weight loss. Considering the simulated regions, kinetic results are presented in three parts.

We first present the results concerning the determination of the activation energy E_a for every mechanism using the Friedman method. Second, the kinetics of the polymer-to-ceramic conversion is examined using the methods proposed by Málek et al.[19] to predict the types of mechanisms (from a physical point of view) that govern the complex solid-state chemical transformation of the poly[*B*-(methylamino)borazine] into boron nitride. Third, the determination of the preexponential factor *A* (Friedman method) is achieved. Taken together, the data allow us to draw conclusions about the energetics of the ceramic conversion and the prediction of the chemical pathways by considering the chemistry of the polymer and using a mechanistic approach.

Activation Energy Determination. The kinetic Friedman method allows for observing the variation of E_a as a function of the conversion and can adapt to multistep reaction schemes.[32] The Friedman plots representing the variation of ln dα/dt as a function of 1/T (eq 5) for the five regions at different heating rates are shown in Figure 9. Each region is represented by two parallel linear fittings (e.g., two conversion degrees) for accuracy in E_a values. It should be mentioned that only five measurements were carried out for the first mechanism instead of six due to the impossibility to distinguish the first region at 20 K min^{-1} (Figure 8).

The Friedman plot indicates a gradual increase of the slope of the straight lines as a function of the extent of conversion. Therefore, the averaged values of E_a deduced from the slope of the two straight lines for every region are seen to increase from region 1 to region 5 (Table 3). Interestingly, Table 3 shows that the Friedman values of E_a for the major mechanisms (second

TABLE 3: Determination of the Activation Energy for Every Mechanism Using the Friedman Method

mechanism	first	second	third	fourth	fifth
E_a (kJ mol^{-1})	38.73 ± 0.64	46.67 ± 0.38	82.73 ± 1.27	124.01 ± 0.38	146.64 ± 2.0

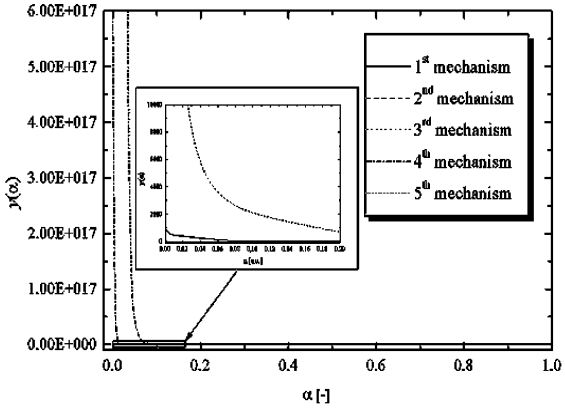

Figure 10. Experimental curve representing the plot of the $y(\alpha)$ function vs α for every one of the mechanisms during the thermal decomposition at 6.4 K min^{-1}.

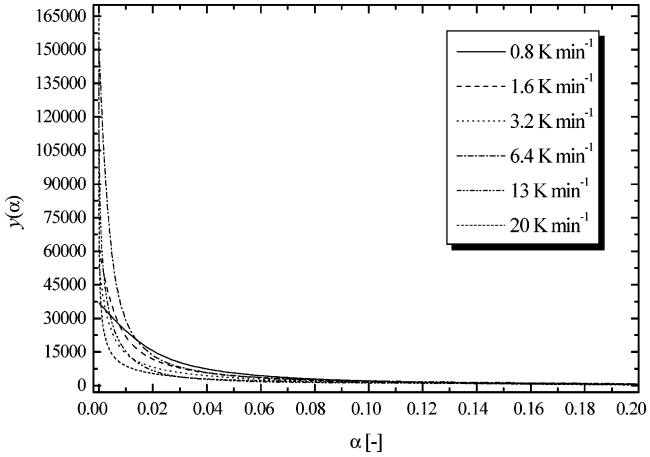

Figure 11. Experimental curves representing the plot of the $y(\alpha)$ function vs α for the second mechanism during the thermal decomposition at six heating rates.

and fourth) are in good agreement with those measured using the Kissinger method (Table 2), suggesting that the deconvolution for the major stages is adequate.

On the basis of data reported in Figure 9 and Table 3, we can assume that the first weight loss is governed by three poorly energetic mechanisms ($\alpha \leq 0.45$), whereas the second weight loss proceeds through two highly energetic mechanisms ($\alpha > 0.45$), suggesting an increase of the complexity of mechanisms with the progress of the ceramic transformation. In reference to such findings, the physical nature of these mechanisms may be studied in the following sections using the methods proposed by Málek et al.[19]

Solid-State Mechanisms. Málek et al. introduced the $y(\alpha)$ and $z(\alpha)$ functions based on both the experimental TG data and the E_a values for plotting curves for each region using eqs 7 and 8 and finally compared experimental curves with reference ones. Obviously, it is expected that the best fitting of an empirical curve by a theoretical one allows the kinetic model associated with the corresponding region to be identified.

For simplification, kinetic plots were reported only for certain heating rates and/or mechanisms, but it should be emphasized that all heating rates and mechanisms were tested and experiments were repeated to reach maximum accuracy.

Figure 10 presents the $y(\alpha)$ kinetic plot of $(d\alpha/dt)\exp(x)$ versus α using eq 7 obtained for every one of the simulated mechanisms recorded at a heating schedule of 6.4 K min^{-1}.

Figure 10 shows that the representative curves of $y(\alpha)$ display identical concave profiles with a maximum value $\alpha_y^{\infty} = 0$ for each mechanism, being invariant with respect to heating rate as highlighted in Figure 11 for the second mechanism.

The concave profile of the experimental curves suggests that experimental data really match theoretical curves, which are based on diffusion-type kinetic models.[19] As a consequence, the conversion of poly[*B*-(methylamino)borazine] into boron nitride is clearly governed by a complex diffusion-controlled thermal process in which every individual transport mechanism is of the deceleration (D_n) type. D_1-, D_2-, D_3-, and D_4-type mechanisms are equally possible only by considering the $y(\alpha)$ function (eq 7).

The nature of the diffusion-controlled transport mechanisms may be clarified using eq 8 based on the definition of the $z(\alpha)$ function. The $z(\alpha)$ method consists of the plot of $1/b(d\alpha/dt)\pi(x)T$ as a function of α in a normalized α interval for every mechanism as represented in Figure 12 for a heating rate of 6.4 K min^{-1}.

Two series of curves are distinguished. The first series (second and fourth mechanisms), composed of a maximum value $\alpha_z^{\infty} \approx 0.704$, is best fitted with reference curves according to D_3-type mechanisms (three-dimensional diffusion; Jander equation[38]). The curve profile even remained almost independent of the heating rate as shown in Figure 13 for the second mechanism.

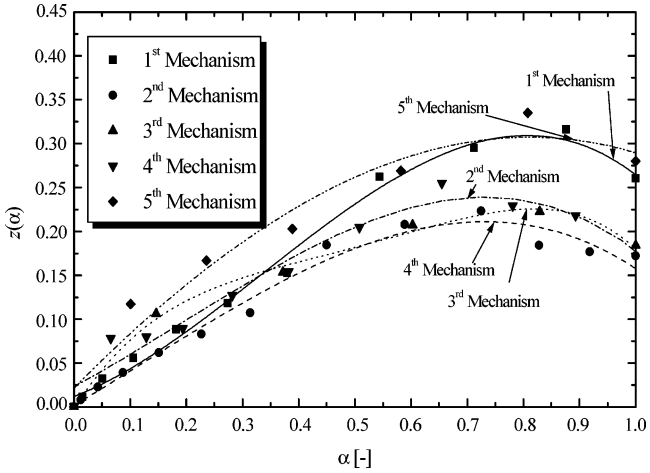

Figure 12. Experimental curves representing the plot of the $z(\alpha)$ function vs α for every one of the mechanisms at 6.4 K min^{-1}.

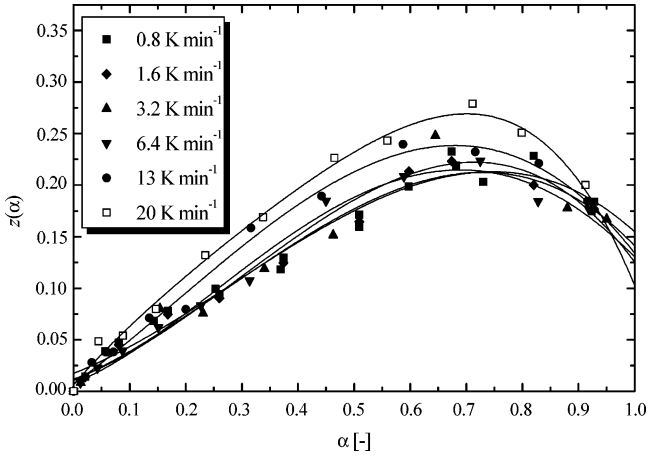

Figure 13. Experimental curves representing the plot of the $z(\alpha)$ function vs α for the second mechanism during the thermal decomposition at six heating rates.

In contrast, it is interesting to note that the second series of curves, which corresponds to minor mechanisms (first, third, and fifth mechanisms), adequately matches reference curves

TABLE 4: Determination of the Logarithm Form of the Preexponential Factor for Every Mechanism Using the Friedman and Second-Derivative Methods

	mechanism	first (D_2)	second (D_3)	third (D_2)	fourth (D_3)	fifth (D_2)
Friedman method	ln *A*	2.68	3.76	10.91	11.70	14.57
second-derivative method		3.68	4.24	12.3	12.85	15.82

based on D_2-type kinetic models with a maximum value of $\alpha_z^\infty \approx 0.834$ (two-dimensional diffusion) being invariant with the increased heating rate. Such findings suggest that the thermal decomposition of poly[*B*-(methylamino)borazine] can be modeled by D_n-type equations in which two- and three-dimensional diffusion-type mechanisms are the rate-limiting steps. These results allow us to determine the preexponential factor *A* associated with every one of these diffusion-type mechanisms.

Preexponential Factor Determination. The preexponential factor *A* is calculated using the Friedman method from the *y*-intercept of the straight Friedman lines (Figure 9) taking into account both the kinetic model function $f(\alpha)$ and the kinetic parameter E_a for every mechanism contributing to the thermal decomposition of the poly[*B*-(methylamino)borazine]. Values of ln *A* are reported in Table 4.

Table 4 highlights that the preexponential factor and the activation energy are mutually correlated, since the values of ln *A* follow the variation of E_a values from region 1 to region 5. However, it should be emphasized that the ln *A* values are derived from the *y*-intercept term of the Friedman plot with a logarithm form, which may produce a large variation in its measurement from a small deviation of values for the *y*-intercept. Therefore, the second-derivative method derived from eq 9 was alternatively used to check the reliability of the Friedman results for each mechanism. Results are reported in Table 4.

Obviously, if results in ln *A* values are corroborating using both equations, then the physical nature of the above-postulated mechanisms can be validated.

Considering the definition of the derivative of $f(\alpha)$ for every mechanism, i.e., $f'(\alpha) = [1/2 - (1 - \alpha)^{-1/3}]/[1 - (1 - \alpha)^{1/3}]^2$ (second and fourth mechanisms) and $f'(\alpha) = -1/[\ln(1 - \alpha)]^2 \cdot (1 - \alpha)$ (first, third, and fifth mechanisms), Table 4 shows that the Friedman and second-derivative methods are in relative good agreement. This points to the fact that both diffusion-type models and values of E_a are validated for every one of the reactions contributing to the thermal transformation of the poly[*B*-(methylamino)borazine] into a solid-state boron nitride material.

Discussion

Results showed that five distinct regions could be identified during the conversion of a typical melt-spinnable poly[*B*-(methylamino)borazine] into boron nitride using the Lorentz fitting approach for the DTG curves at various heating rates. As an illustration, it is shown that the first weight loss ($0 \le \alpha \le 0.45$) is associated with three parallel poorly energetic mechanisms, whereas the fourth and fifth stages, which weakly overlap each other, compose the second weight loss and are highly energetic ($0.45 < \alpha \le 1$). This polymer-to-ceramic transformation process is characterized by diffusion-controlled transport mechanisms and a large two-step evolution of methylamine.

It is widely demonstrated that the PDCs are prepared through a cross-linking/curing process followed by a thermolysis step including the mineralization and ceramization processes.[4] Considering the values of kinetic parameters, the physical nature of the solid-state transport mechanisms and the average bond energies of various bonds present in the polymeric precursor, we can discuss these cross-linking, mineralization, and ceramization processes using a mechanistic approach.

SCHEME 1: Postulated Structure of Poly[*B*-(methylamino)borazine] ($[B_{3.0}N_{4.6}C_{2.1}H_{9.5}]_n$, $n \approx 7$)

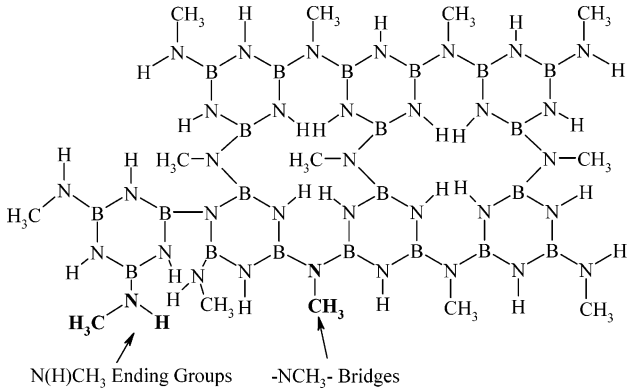

Cross-Linking Process. The first weight loss associated with regions one, two, and three likely corresponds to a cross-linking process of the polymer network. It is shown in Table 3 that these regions give the lowest values of E_a. As a consequence, since the dissociation energy of the intraring B−N bond in a borazine ring is as high as 501 kJ mol^{-1}, it is expected that these three mechanisms do not affect the borazine molecular unit in the poly[*B*-(methylamino)borazine].[39] This can be understood by considering the idealized structure of the poly[*B*-(methylamino)borazine] ($[B_{3.0}N_{4.6}C_{2.1}H_{9.5}]_n$). Ideally, it represents a melt-spinnable polymer composed of a small repetition of monomeric units ($n \approx 7$), which is cross-linked via a majority of $-N(CH_3)-$ bridges connecting borazine rings together.[35,36] It is composed of residual $-N(H)CH_3$ end groups due to an incomplete condensation reaction. A conceptual schematic for the molecular network of such a polymer based on elemental analysis and IR and liquid-state NMR spectroscopies is illustrated in Scheme 1.

It should be mentioned that a low proportion of NH_2/NH groups as well as inter-ring B−N bonds connecting two borazine rings are likely present in the basal structural unit of the polymer.[35−36]

In the first regions, GC curves (Figure 3) and infrared spectra (Figure 14) showed a liberation of methylamine (disappearance of methyl-based groups in the polymer structure; 2954−2816 cm^{-1} (ν; FT-IR)) from the heated polymer. Besides, IR spectra

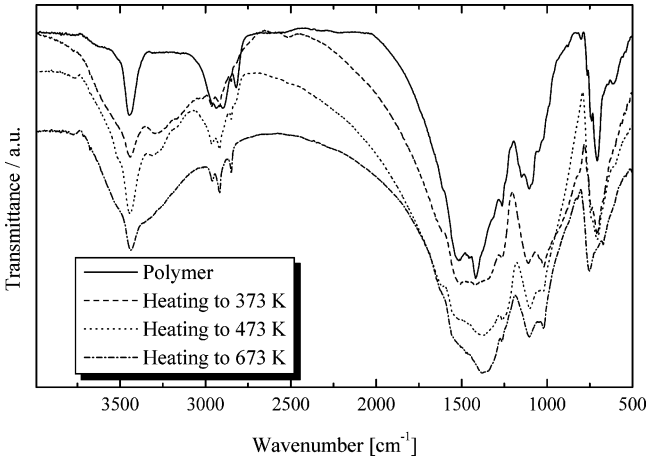

Figure 14. Infrared spectra (FT-IR) of intermediates isolated during the cross-linking process of the poly[*B*-(methylamino)borazine] at 6.4 K min^{-1}.

SCHEME 2: Proposed Mechanisms during Region One

Ammonolysis Reaction (Amine-exchange Process) during Region One

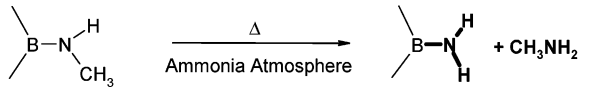

SCHEME 3: Proposed Mechanisms during Region Two

Condensation Reaction of Ending Groups during Region Two

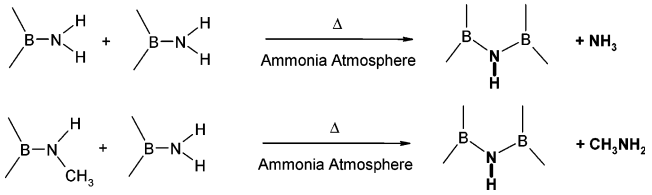

SCHEME 4: Proposed Mechanisms during Region Three

Condensation Reaction of $B_2N(H)$ sites during Region Three

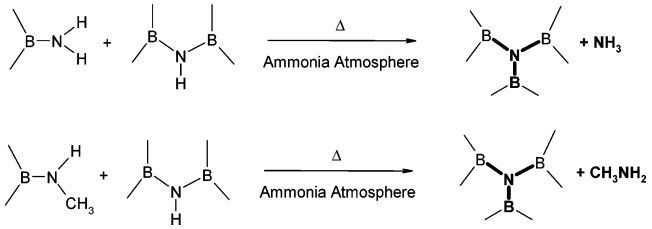

show that this evolution of methylamine is accompanied by the appearance of $-NH_2$ groups and/or N(H) units in the ranges 1000−1150 cm^{-1} and 3000−3500 cm^{-1} (FT-IR).

These findings may support the conclusion that the cross-linking process predominantly represents amine-exchange reactions followed by condensation metathesis.

Initially, as the poly[*B*-(methylamino)borazine] is heated in an ammonia atmosphere at low temperature ($T \approx 323-333$ K (0.8 K min^{-1}); $\alpha = 0.02-0.025$), a first heating zone is reached where the thermal energy is sufficient to activate ammonolysis reactions of $-N(H)CH_3$ ending groups as illustrated in Scheme 2.

The $-N(H)CH_3$ ending group is seen as a very good leaving group through the diffusion of ammonia in the polymer network, so that a low energy input is sufficient to decompose and replace $-N(H)CH_3$ groups by more reactive $-NH_2$ groups leading to the evolution of methylamine (CH_3NH_2; Figure 3). The structure of the polymeric network therefore changes to activate facile condensation reactions in regions two and three.

Regions two and three are expected to have a higher E_a than region one, since the mechanisms in these regions are a continuation of what previously occurred at low temperatures during the first stage (Schemes 3 and 4).

While region one occurs with ammonolysis reactions (amine-exchange process; Scheme 2), controlled condensations reactions of as-formed highly reactive $-NH_2$ end groups and disappearing $-N(H)CH_3$ end groups take place almost simultaneously. The condensation of such groups results in the building of an extended network cross-linked via new inter-ring bridging $-N(H)-$ species in region two as depicted in Scheme 3.

Large amounts of gaseous byproducts such as methylamine diffuse out from the polymeric structure in the second region. It is expected that ammonia (reactions between two $B-NH_2$ units) is also produced in this region,[35] but it cannot be identified by GC experiments due to the use of an ammonia atmosphere during TG experiments.

The presence of N(H) units in the basal borazine ring and the formation of bridging $-N(H)-$ groups provide one plausible route for developing a reaction pathway in the third region. A heating zone at the higher temperature characterizing the region three is reached where there is enough thermal energy to break N−H bonds in more thermally stable borazinic N(H) units as well as in as-formed bridged $-N(H)-$ groups. Their reaction with end groups allows for further cross-linking, resulting in the development of tertiary NB_3 sites between the poly[*B*-(methylamino)borazine] chains and additional formation of methylamine (reaction between one B−N(H) unit and one $B-N(H)CH_3$ unit) and ammonia reaction between one B−N(H) unit and one $B-NH_2$ unit) as illustrated in Scheme 4.

Schemes 3 and 4 demonstrate that regions two and three play an important part in the cross-linkage of the polymeric system, leading to cross-linked $-N(H)-$ bridges and NB_3 sites and therefore to branched-chain formation.

The gradually cross-linked preceramic network is finally transformed into boron nitride through mineralization (fourth step) and ceramization (fifth step) processes. Such processes, which are mainly activated during the second weight loss, must thereby include a series of controllable reactions, which are aimed for the specific architecture (hexagonal) of the boron nitride material.

It should be understood that boron nitride is characterized by a repetition of fused six-membered rings (hexagons) in the three dimensions as a "naphthalenic-type structure" free of carbon and hydrogen elements.[40] Considering the idealized structure of the poly[*B*-(methylamino)borazine] (Scheme 1), mineralization and ceramization processes should be governed by structural rearrangements involving the formation of fused-cyclic borazines and the removal of carbon- and hydrogen-based gaseous species.

Producing fused-cyclic borazine from highly cross-linked poly[*B*-(methylamino)borazine] chains is a very energetic process, since it induces the cleavage of a boron−nitrogen bond followed by the building of fused six-membered rings.

Mineralization Process. Taking into account that methylamine is identified as a significant byproduct in region four by GC experiments (Figure 3), it is reasonable to suggest that the evolution of such a gaseous byproduct may be due to the decomposition of bridging $-N(CH_3)-$ units. This occurs by the cleavage of the inter-ring boron−nitrogen bond to subsequently form $-N(H)CH_3/-NH_2$ end groups. Such good leaving groups are enabled to form fused rings by the cleavage of the intraring B−N bonds according to the proposed mechanism depicted in Scheme 5.

IR experiments up to 1273 K (6.4 K min^{-1}) highly reflect such reasoning (Figures 14 and 15).

As the stability of a chemical bond depends primarily on its bond energy, the cleavage of the intraring boron−nitrogen bond, which is the strongest bond present in the polymer[39] (D_{B-N} = 501 kJ mol^{-1}), requires high temperature in good agreement with the temperature range where the mechanism associated with region four is activated.

Ceramization Process. Region five, which characterizes the end of the decomposition which leads to boron nitride, represents a continuation of what previously started (mineralization). However, the mechanism associated with region five is the most complex, since it is most likely that mechanism 5 is associated with successive cleavages of intraring B−N bonds and rearrangements to form the boron nitride structure through a low ammonia loss. Scheme 6 proposes a summarized ideal mechanism. The highest E_a value in region five suggests that the

SCHEME 5: Proposed Mechanisms during Region Four

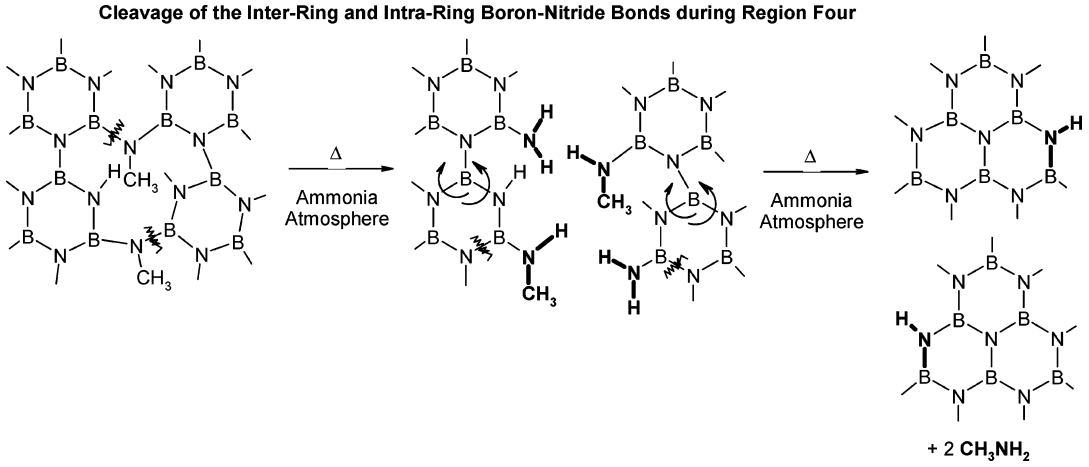

SCHEME 6: Proposed Mechanisms during Region Five

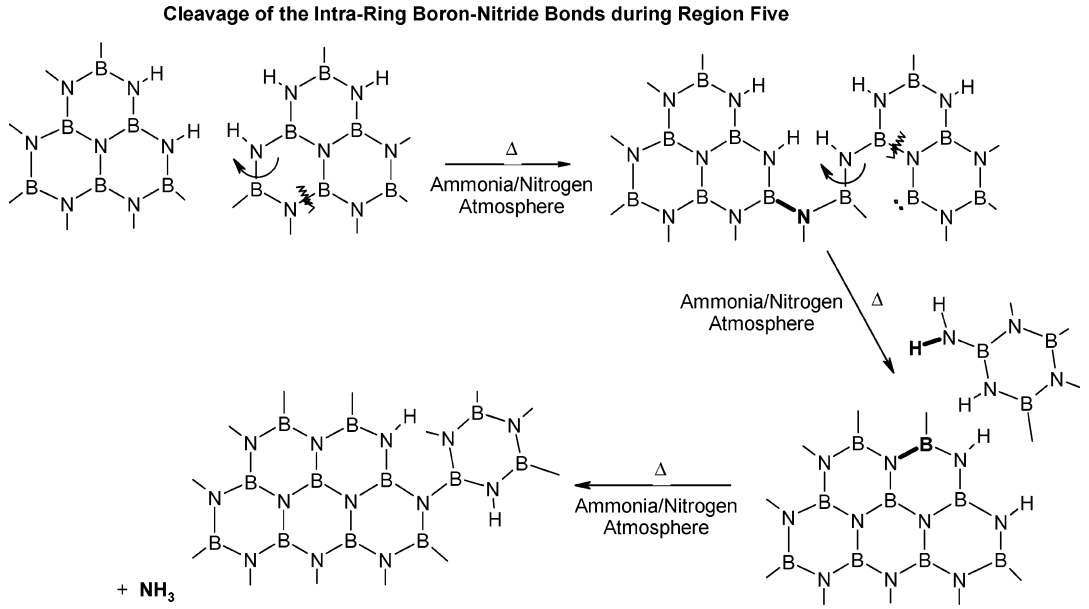

cleavage of the intraring B−N bonds is the rate-controlling step for this process.

Diffusion-Type Mechanisms. The increase in activation energy from region one in going to region five indicates that the mechanisms within those regions are parallel routes to the formation of boron nitride fibers from poly[*B*-(methylamino)-borazine]. Furthermore, regions four and five display the highest E_a values, because there is a comparison of several energetic processes in such regions (second weight loss) to one for the regions in the first weight loss (first, second, and third regions).

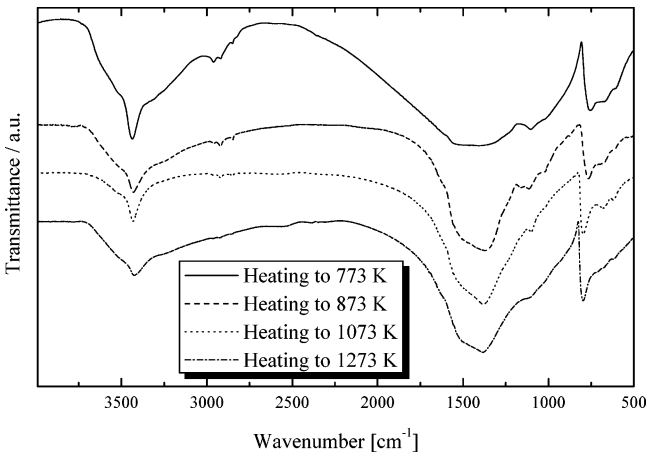

Figure 15. Infrared spectra (FT-IR) of intermediates isolated during the mineralization and ceramization processes of the poly[*B*-(methylamino)borazine] at 6.4 K min^{-1}.

During the thermal decomposition of the polymer, methylamine and ammonia are assumed to be formed by the previously depicted chemical reactions, so that these gases probably diffuse from the reactional site (−N(H)CH_3 and −NH_2 end groups as well as bridged −N(H)− and −N(CH_3)− units) where they are evolved to the surface of the material. We therefore suggest that the intervening mechanisms between the solid-phase generation of gases and gas-phase transport involve a process of adsorption (ammonia atmosphere) and desorption (removal of gas) from the solid. In this connection, it is clear that the best transport models, in terms of the minimum deviation between theoretical and experimental data and from the standpoint of physical/chemical sense, are therefore of the diffusion type.

Let us consider that the poly[*B*-(methylamino)borazine] undergoes a complex thermal decomposition process that

SCHEME 7: Flow Diagram for the Preparation of PDCs through the Preparation of Poly[*B*-(methylamino)borazine]-Derived Boron Nitride Fibers

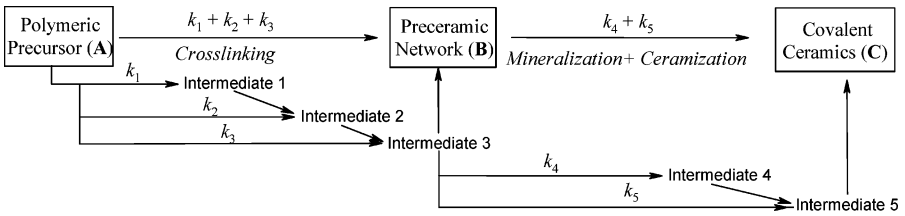

SCHEME 8: Two-Step Simplified Thermal Decomposition of the Poly[*B*-(methylamino)borazine]

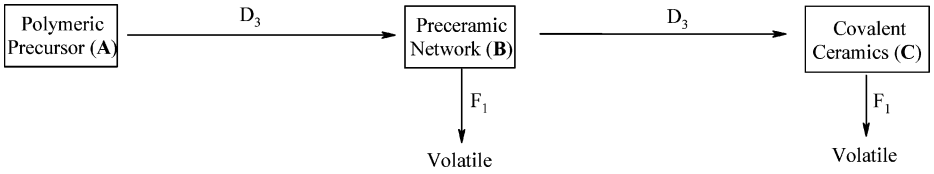

consists of overlapping reactions, each reaction leading to a solid intermediate and gaseous species. An illustration of the five-step conversion of the poly[*B*-(methylamino)borazine] (A) into boron nitride (C) through a solid intermediate B is illustrated in Scheme 7. It should be mentioned that the pyrolysis intermediates from 1 to 4 in Scheme 7 cannot be isolated, since they continuously change with the increased temperature.

Model Simulation. Here, we are interested in determining if both our kinetic parameters and our kinetic models for the conversion of the poly[*B*-(methylamino)borazine] into boron nitride may predict the weight loss data with respect to temperature. It is important to mention here that, due to the complexity of the polymer-to-ceramic conversion, a model reconstruction for the TG data has not been performed through the five processes. It is always possible to make the system more complex by including all five steps, but the aim in this section is to obtain a representation as simple as possible to describe the process producing accurate results. Hence, we have reduced our study to the two main peaks obtained from DTG data (Figure 4) applying Lorentz deconvolution on them as shown in Figure 16 for a heating rate of 6.4 K min^{-1}.

We assume a pseudo-mechanism in two global steps, in which every one of the reactions is composed by the different processes identified from the DTG curves. The first step starting from A (identified in Scheme 7 as the polymeric precursor) leads to an intermediate compound B comparable to a highly cross-linked solid (Scheme 7). In the second stage, the intermediate product B is transformed into a ceramic product C (Scheme 7). This concept was built around the two major mechanisms (steps 2 and 4).

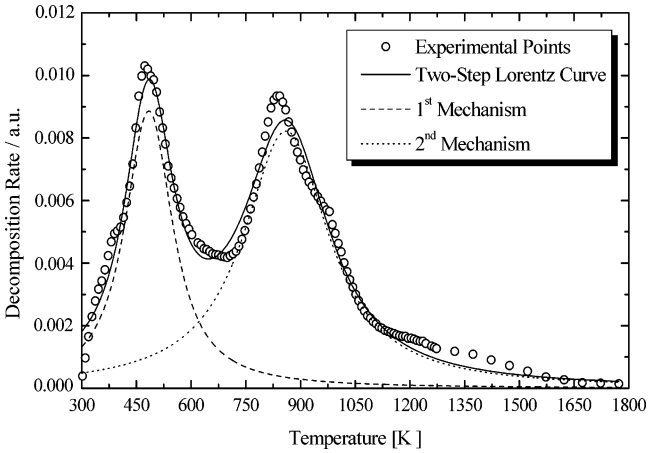

Figure 16. Simulation of the experimental DTG curve (0.8 K min^{-1}) using two Lorentz peaks.

Several reaction models were selected, but it is interesting to assume that the simulated curves really match the experimental TG profiles by introducing a modified D_3-type mechanism expressed by eq 11 for both the steps, assuming two global independent reactions

$$\frac{d\alpha}{dT} = \frac{k_1(T)}{b}\frac{3(1-\alpha)^{2/3}}{2[1-(1-\alpha)^{1/3}]} - \frac{k_2(T)}{b}\alpha \qquad (11)$$

This means that the weight loss rate is a sum of the decomposition rate evolved by the primary process A $\rightarrow$ B and a decomposition rate of a fraction of B due to partial volatilization of gaseous byproducts, as shown in Scheme 8.

The two processes can be traduced in eqs 12 and 13

$$\frac{d\alpha_1}{dT} = \frac{k_{11}(T)}{b}\frac{3(1-\alpha_1)^{2/3}}{2[1-(1-\alpha_1)^{1/3}]} - \frac{k_{21}(T)}{b}\alpha_1 \qquad (12)$$

$$\frac{d\alpha_2}{dT} = \frac{k_{12}(T)}{b}\frac{3(1-\alpha_2)^{2/3}}{2[1-(1-\alpha_2)^{1/3}]} - \frac{k_{22}(T)}{b}\alpha_2 \qquad (13)$$

where $k_{ij}(T) = A_{ij}\exp(-E_{aij}/RT)$ with i and $j = 1$ or 2.

It is relevant to mention here that, even if we assume two main single steps for sake of simplicity, every step does not necessarily mean that the decomposition reaction is a single process. The overall mass loss was then expressed through eq 14

$$\frac{d\alpha}{dT} = \frac{d\alpha_1}{dT} + \frac{d\alpha_2}{dT} \qquad (14)$$

To calculate the kinetics parameters, an adjustment to the experimental data by nonlinear least-squares regression was carried out. A modified Levendberg−Marquardt algorithm from Matlab software was used. The fitting was done separately on experiments at 0.8 and 20 K min^{-1}. The results are reported in Table 5. It should be mentioned that values were averaged for simulation.

The kinetic results show that the averaged values of E_a (Table 5) in the first step are close to the values of the major mechanism reported in Tables 2 and 3, while, in the second step, the results

TABLE 5: Determination of the E_a and ln A Values for the Major Mechanism Using a Modified Levendberg−Marquardt Algorithm from Matlab Software

	kinetic parameters			
	E_{aij} (kJ mol^{-1})	$\overline{E_{aij}}$ (kJ mol^{-1})	ln A_{ij}	ln $\overline{A_{ij}}$
first step	$45.467 < E_{a11} < 46.284$	$\overline{E_{a11}} = 45.875$	$4.2279 < \ln A_{12} < 4.2913$	$\ln \overline{A_{12}} = 4.260$
	$42.909 < E_{a21} < 45.551$	$\overline{E_{a21}} = 44.232$	$7.2642 < \ln A_{21} < 7.5227$	$\ln \overline{A_{21}} = 7.4018$
second step	$70.449 < E_{a12} < 75.981$	$\overline{E_{a12}} = 73.215$	$3.2683 < \ln A_{12} < 3.4888$	$\ln \overline{A_{21}} = 3.3847$
	$59.001 < E_{a22} < 65.626$	$\overline{E_{a22}} = 62.315$	$3.7588 < \ln A_{22} < 4.0138$	$\ln \overline{A_{22}} = 3.8944$

are closer to the values of the step 3 (Table 3). This means that step 3 tends to affect the kinetic parameter of the main mechanism in the second weight loss in the simplified representation that we have proposed.

We have used a formal resolution of eqs 12 and 13 with Matlab software. The ordinary differential equation system was solved with the averaged values reported in Table 5. The resulting conversion degree was simulated on the whole temperature domain. Simulation was reported for a heating rate at 6.4 K min^{-1}, but it should be underlined that simulations were tested and validated for all experiment heating rates. Figure 17 shows the comparison between the total simulated conversion and the experimental one at 6.4 K min^{-1}. It can be seen that the simulation matches all our experimental data.

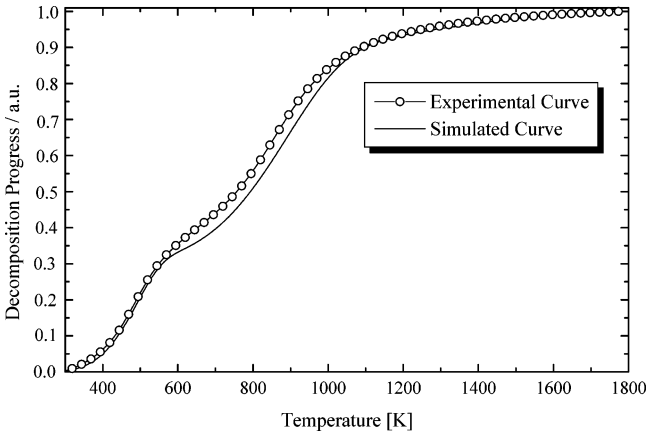

Figure 17. Simulated and experimental curves of the poly[*B*-(methylamino)borazine] as a function of the temperature during TG experiment at 6.4 K min^{-1}.

As a consequence of the ceramic transformation of the poly-[*B*-(methylamino)borazine], the molecular polymer structure (Scheme 1) transforms into a ceramic network through eqs 12−14 according to the simple reaction depicted in Scheme 8.

It should be mentioned that kinetic expression was derived through simplified modeling. Although this model predicted very well the experimental data, a more detailed picture of the kinetic investigation is in progress to study the effect of every one of the five steps mentioned in the present paper through the whole process.

Conclusion

The kinetics of the thermal decomposition of melt-spinnable poly[*B*-(methylamino)borazines] to boron nitride performed under controlled atmospheres (ammonia and nitrogen) is described by means of thermogravimetric analysis via multiple heating rate kinetic models. The combination of these approaches allowed insights into the kinetic parameters and predictions of the physical chemistry nature of the reaction pathways to be obtained. Kinetic parameters (activation energy E_a and preexponential factor ln A) have been determined by the Friedman method and validated by alternative methods. It is shown that heating rate has no effect on the mechanism, but the increase in E_a and ln A values with the increased temperature from region one (E_a = 38.73 kJ mol^{-1}) to region five (E_a = 146.64 kJ mol^{-1}) indicates that the five diffusion-controlled transport mechanisms lead to the formation of boron nitride fibers.

The three-step cross-linking process is activated by ammonolysis reactions that modify the polymeric structure by an incorporation of thermally reactive $-NH_2$ groups through adsorption of ammonia in region one. This allows the occurrence of condensation reactions with a large diffusion of methylamine from the reaction sites to the surface of the material in regions two and three. The latter are responsible for the increase in cross-linking density of the poly[*B*-(methylamino)borazine].

Mechanisms in mineralization (region four) and ceramization (region five) steps represent very energetic processes, since they include a complex sequence of physical and chemical changes through controllable structural rearrangements and condensation steps (chain scission, segment branching). Mechanisms occurred the planar consolidation of the fused six-membered rings in the high-temperature regimes leading to the formation of hexagonal boron nitride through diffusion of methylamine and ammonia. Finally, a kinetic expression has been derived by a simplified modeling that appropriately predicted experimental data.

References and Notes

(1) Wynne, K. J.; Rice, R. W. *Annu. Rev. Mater. Sci.* **1984**, *14*, 297−334.
(2) Blum, Y. D.; Schwartz, K. B.; Laine, R. M. *J. Mater. Sci.* **1989**, *24*, 1707−1718.
(3) Peuckert, M.; Vaahs, T.; Brück, M. *Adv. Mater.* **1990**, *2*, 398−404.
(4) Bill, J.; Aldinger, F. *Adv. Mater.* **1995**, *7*, 775−787.
(5) Greil, P. *Adv. Eng. Mater.* **2000**, 339−348.
(6) KiON Ceraset Polysilazane is a commercially available product of KiON Corporation, PA.
(7) PCS is a commercially available product of Nippon Carbon Ltd.; type S, Tokyo, Japan.
(8) PHPS is a commercially available product of Tonen Co., N-N110, Tokyo, Japan.
(9) Wideman, T.; Cortez, E.; Remsen, E. E.; Zank, G. A.; Caroll, P. J.; Sneddon, L. G. *Chem. Mater.* **1997**, *9*, 2218−2230.
(10) Zheng, Z.; Li, Y.; Luo, Y.; Su, S.; Zhang, Z.; Yang, S.; Gao, W.; Xie, Z. *J. Appl. Polym. Sci.* **2004**, *92*, 2733−2739.
(11) Bernard, S.; Weinmann, M.; Gerstel, P.; Miele, P.; Aldinger, F. *J. Mater. Chem.* **2005**, *15*, 289−299.
(12) Pielichowski, K.; Hamerton, I. *Polymer* **1998**, *39*, 241−244.
(13) Plawsky, J. L.; Wang, F.; Gill, W. N. *AIChE J.* **2002**, *48*, 2315−2323.
(14) Liu, B.; Zhao, X.; Wang, X.; Wang, F. *J. Appl. Polym. Sci.* **2003**, *90*, 947−953.
(15) Numez, L.; Fraga, F.; Numez, M. R.; Villanueva, M. *Polymer* **2000**, *41*, 4635−4641.
(16) Jordan, K. J.; Suib, S. L.; Koberstein, J. T. *J. Phys. Chem. B* **2001**, *105*, 3174−3181.
(17) Sanders, J. P.; Gallagher, P. K. *J. Therm. Anal. Calorim.* **2003**, *72*, 777−789.
(18) Criado, J. M.; Malek, J.; Ortega, A. *Thermochim. Acta* **1989**, *147*, 377−385.

(19) Malek, J. *Thermochim. Acta* **1992**, *200*, 257−269.
(20) Koga, N.; Malek, J. *Thermochim. Acta* **1996**, *282/283*, 69−80.
(21) Ortega, A. *Int. J. Chem. Kinet.* **2001**, *33*, 343−53.
(22) Malek, J.; Mitsuhashi, T.; Criado, J. M. *J. Mater. Res.* **2001**, *16*, 1862−1871.
(23) Ortega, A. *Int. J. Chem. Kinet.* **2002**, *34*, 193−208.
(24) Perez-Maqueda, L. A.; Criado, J. M.; Gotor, F. J.; Malek, J.; Koga, N. *J. Phys. Chem. A* **2002**, *106*, 2862−2868.
(25) Criado, J. M.; Perez-Maqueda, L. A.; Gotor, F. J.; Malek, J. *J. Therm. Anal. Calorim.* **2003**, *72*, 901−906.
(26) Galwey, A. K.; Brown, M. E. *Thermal Decomposition of Ionic Solids*; Elsevier: Amsterdam, 1999.
(27) Bernard, S.; Chassagneux, F.; Berthet, M. P.; Vincent, H.; Bouix, J. *J. Eur. Ceram. Soc.* **2002**, *22*, 2047−2059.
(28) Schmidt, L. D. *The Engineering of Chemical Reactions*; Oxford University Press: New York, 1998.
(29) Brown, M. E.; Dollimore, D.; Galwey, A. K. In *Reactions in the Solid State*; Bamford, C. H., Tipper, C. F. H., Eds.; Comprehensive Chemical Kinetics 22; Elsevier: Amsterdam, 1980; p 340.
(30) Galwey, A. K.; Brown, M. E. *Thermochim. Acta* **2002**, *386*, 91−98.
(31) Kissinger, H. E. *Anal. Chem.* **1957**, *29*, 1702−1706.
(32) Friedman, H. L. *J. Polym. Sci.* **1963**, *6*, 183−195.
(33) Koga, N.; Sestak, J.; Malek, J. *Thermochim. Acta* **1991**, *188*, 333−336.
(34) Koga, N.; Sestak, J. *J. Therm. Anal.* **1991**, *203*, 1103−1108.
(35) Duperrier, S.; Bernard, S.; Gervais, C.; Cornu, D.; Babonneau, F.; Miele, P. *J. Mater. Chem.*, submitted for publication.
(36) Duperrier, S.; Bernard, S.; Chiriac, R.; Sigala, C.; Cornu, D.; Miele, P.; Balan, C.; Gervais, C., to be submitted for publication.
(37) Breit, G.; Wigner, E. *Phys. Rev.* **1936**, *49*, 519−531.
(38) Jander, W. *Z. Anorg. Allg. Chem.* **1927**, *163*, 1−30.
(39) Cote, M.; Haynes, P. D.; Molteni, C. *Phys. Rev. B* **2001**, *63*, 125207.
(40) Paine, R. T.; Narula, C. K. *Chem. Rev.* **1990**, *90*, 73−91.